RSC Advances

PAPER

View Article Online
View Journal | View Issue

Cite this: *RSC Adv.*, 2015, **5**, 6588

A facile strategy to achieve high conduction and excellent chemical stability of lithium solid electrolytes†

Shufeng Song, Jia Lu, Feng Zheng, Hai M. Duong and Li Lu*

Received 26th September 2014
Accepted 17th December 2014

DOI: 10.1039/c4ra11287c

www.rsc.org/advances

Lithium solid electrolytes have shown their potential for high-energy density batteries. The use of solid electrolytes will also be able to overcome safety issues associated with conventional carbonate-based electrolytes. However, achieving the combination of high ionic conductivity and excellent electrochemical stability in lithium solid electrolytes is still a major challenge. Herein we report a facile strategy to achieve high conduction and excellent electrochemical stability by the substitution of Cl for O based on the concept of bottleneck size and binding energy. The ionic conductivities of $Li_{10.42}Si_{1.5}P_{1.5}Cl_{0.08}O_{11.92}$ and $Li_{10.42}Ge_{1.5}P_{1.5}Cl_{0.08}O_{11.92}$ are 1.03×10^{-5} S cm^{-1} and 3.7×10^{-5} S cm^{-1} at 27 °C, respectively, which are 13 orders of magnitude higher than that of the pure Li_3PO_4, and 1 order of magnitude higher than that of the pristine $Li_{10.5}Si_{1.5}P_{1.5}O_{12}$. The electrochemical stability with metallic lithium is up to 9 V *vs.* Li^+/Li, which is one of the widest electrochemical windows of solid electrolytes. This research also addresses the crystal structure, lithium ion migration mechanism, and battery performance.

Introduction

Although lithium-ion batteries are now widely used in many electronic products, safety, energy density, and service life are still issues, which continue to plague lithium-ion batteries for the potential of mass market of electric vehicles and large-scale energy storage.[1] There are two ways to increase the energy density, one of which is to increase the specific capacity and the other one is to increase the voltage potential of the cathode which is limited by current liquid electrolytes. Applying solid electrolytes to lithium batteries will eliminate the conventional voltage limitation (4.5 V *vs.* Li^+/Li) of currently used carbonate-based electrolytes and open up the possibility of high-voltage operation with 5 V-class cathode materials.[2] On the other hand, metallic lithium batteries exhibit the highest theoretical energy densities. Among many possible systems, Li–S and Li–O_2 batteries are very attractive as candidates for next-generation high-energy density batteries. The use of solid electrolytes could potentially suppress the formation of lithium dendrites, that are caused by uneven current distributions at the metal–electrolyte interface during cycling.[3]

A number of works reported new solid electrolytes, such as sulfide-based superionic conductors.[4] Recently, a breakthrough has been achieved in inorganic sulfide-based electrolyte with extremely high room temperature conductivity of 10^{-2} S cm^{-1}.[5,6] Generally, sulfides have higher ionic conductivity than oxides but lower air and moisture stability than oxides. The hypersensitivity of the sulfides to air and moisture requires sophistically and tedious treatment procedures under dry inert gas atmosphere, which increase their processing cost.[7] Moreover, the sulfides suffer inferior electrochemical stability due to reacting continuously with Li anode.[8] In an effort to overcome inferior electrochemical stability, the lithium phosphorous oxynitride (LPON) electrolyte developed at Oak Ridge National Laboratories (ORNL) exemplifies the extremely good stability with Li metal anode. The ORNL group reports thin film batteries employing the LPON electrolyte, $LiCoO_2$ cathode, and Li metal anode are capable of over 20 000 charge–discharge cycles with 0.001% capacity loss per cycle. Unfortunately LPON has relatively poor ionic conductivity of *ca.* 2×10^{-6} S cm^{-1}.[9]

Although the advantages of non-flammable solid electrolytes are widely acknowledged, their low ionic conductivities or low chemical and electrochemical stabilities prevent them from practical applications. It is known that the ionic conductivity is given by:

$$\sigma = Zen\mu \quad (1)$$

where, Ze is the ionic charge, n is the carrier concentration and μ is the mobility of the ion. The mobility of the ions mainly depends on the activation energy for ion conduction.[10] To migrate from one site to next available one, the lithium ions

Department of Mechanical Engineering, National University of Singapore, 9 Engineering Drive 1, Singapore 117576, Singapore. E-mail: luli@nus.edu.sg; Fax: +65-67791459; Tel: +65-65162236

† Electronic supplementary information (ESI) available. See DOI: 10.1039/c4ra11287c

have to pass through a bottleneck consisting of four oxygen ions. The bottleneck size is the predominant factor of the activation energy.[11] As predicted by Inaguma *et al.*,[12] the size of the bottleneck mostly influences the activation energy of the ionic conduction by varying the repulsion potential between oxygen and lithium at the bottleneck site. Ion mobility is physically governed by the bottleneck size and chemically by the binding energy between mobile ions and the network anions. The suitable bottleneck size should be favor of ions conduction, while the covalent bonding between the mobile ion and network anion should be weak as possible.[13] The present paper reports a facile method to improve ionic conductivity of oxides while maintaining their chemical stability with air and moisture and electrochemical stability with Li metal anode. To demonstrate the concept discussed above, the solid solutions of Li_3PO_4 and Li_4Si/GeO_4 are selected as prototype material by considering their good stability, while the halide elements (F, Cl, Br) are selected to partly substitute O ions to adjust the bottleneck size and binding energy, in order to improve the ionic conductivity, considering the higher electronegativity of F than O, and larger ionic radii of Cl and Br than O. Two issues will be addressed in this work: (1) is substitution of halide elements for oxygen valid strategy to enhance the ionic conductivity of oxides? (2) Dose the halide-oxides have the expected electrochemical stability with Li metal? This research also addresses the crystal structure, lithium ions migration mechanism, and battery performance of the halide-oxides materials.

Experimental

Synthesis of halide-substituted solid solutions of Li_3PO_4 and Li_4Si/GeO_4 [$Li_{10.5-x}Si/Ge_{1.5}P_{1.5}Cl_xO_{12-x}$ ($0.05 \leq x \leq 1.0$)]

$Li_{10.5-x}Si/Ge_{1.5}P_{1.5}Cl_xO_{12-x}$ ($0.05 \leq x \leq 1.0$) was prepared by melt-casting method. All the raw materials were received from Sigma, and the stoichiometric amounts of Li_2CO_3 (99%, with 5 wt% excess to compensate for the loss of lithium during melting), SiO_2 (99%), GeO_2 (99.999%), $NH_4H_2PO_4$ (98.5%), LiCl (99%), LiF (99%), and LiBr (99%) were weighed and ball-milled using zirconia balls for about 2 h in industrious ethanol in air. The mixed materials were pre-calcined at 700 °C for 2 h, subsequently, the calcined powder was melted at 1200–1250 °C, the sheet with thickness of about 1 mm was obtained after casting the melt using a rolling machine. For some specific samples, the F and Br were added to study their effects on ionic conductivity. Although the materials are not air-sensitive, to avoid possible interference from absorbed moisture, all the casted sheets were immediately transferred into an argon-filled glove box.

Electrochemical characterization

For the ionic conductivity measurements, the sheets were cut to small pellet and the conducting silver paste was painted on both sides of the small sheet and sealed in a Swagelok cell. Electrochemical impedance spectroscopy (EIS) measurements were carried out using a Solartron 1260 + 1287 System, applying 100 mV in the frequency range 1 MHz–10 Hz, without any pressure applied. Activation energy was measured at the temperature range from 27 °C to 110 °C.

Cyclic voltammogram (CV) of the samples made of Ag\$Li_{10.42}Si/Ge_{1.5}P_{1.5}Cl_{0.08}O_{11.92}$ sheet\Li was measured using a linear sweep voltammetry between a voltage range from −0.5 V to 9 V *vs.* Li^+/Li at a 1 mV s^{-1} scan rate.

Full cells using $Li_{10.42}Si/Ge_{1.5}P_{1.5}Cl_{0.08}O_{11.92}$ as the electrolytes, $0.3Li_2MnO_3 \cdot 0.7LiMn_{1.5}Ni_{0.5}O_4$ as the cathode and lithium metal as the anode were assembled in 2025 coin cells. The cathode powder was mixed with super P conductive carbon (TIMCAL Ltd.) and polyvinylidene fluoride (PVDF, Sigma) at a weight ratio of 8 : 1 : 1 in an *N*-methylpyrrolildone (NMP, Sigma) solvent to form uniform slurries and then coated on Al foils. To reduce interfacial impedance between the cathodes and electrolytes, a very little drop of 1 M $LiPF_6$ in EC–DEC (1 : 1 by weight) as a buffer between solid electrolyte and cathode layer. Charge–discharge test was performed at a potential range between 2.0 and 5.0 V *vs.* Li^+/Li at 0.1 C rate.

Structural characterization

X-ray diffraction (Shimadzu XRD-6000 and 7000 Cu-Kα) was employed to detect crystallographic structure of the samples in air with no seal. Lattice constants and structures were analyzed by Rietveld refinement of the powder XRD data using GSAS software. The structure was drawn by VESTA software.

Results and discussion

Fig. 1 represents typical Nyquist plots of $Li_{10.42}Si_{1.5}P_{1.5}Cl_{0.08}O_{11.92}$ (square symbol) and $Li_{10.42}Ge_{1.5}P_{1.5}Cl_{0.08}O_{11.92}$ (circle symbol) measured at 27 °C. It shows a depressed rather than ideal semicircle, inclined rather than vertical capacitive tail. The appearance of the tail at low frequencies in the case of ionically blocking electrodes is an indication that the pellet is ionically conducting in nature.[14] Close examination of the Nyquist plot, there is only one semicircle, suggesting that the grain and grain boundary resistance be unable separated. The total conductivity of the pellet at 27 °C is calculated by the equation:

$$\sigma_t = \frac{1}{R_t}\frac{d}{S} \quad (2)$$

where R_t, d, S are the total resistance, the thickness of sample, the electrode area, respectively. For the sample ($d = 1.0$ mm, $S = 28.3$ mm^2), the total conductivity of $Li_{10.42}Si_{1.5}P_{1.5}Cl_{0.08}O_{11.92}$ at 27 °C is calculated to be 1.03×10^{-5} S cm^{-1}, which is 13 orders of magnitude higher than that of the pure Li_3PO_4 (10^{-18} S cm^{-1}),[15] and 1 order of magnitude higher than that of the pristine $Li_{10.5}Si_{1.5}P_{1.5}O_{12}$ (10^{-6} S cm^{-1}),[4,16] and the room-temperature conductivity of its counterpart $Li_{10.42}Ge_{1.5}P_{1.5}Cl_{0.08}O_{11.92}$ is much higher with 3.7×10^{-5} S cm^{-1}.

Fig. 2 shows the Arrhenius plots of $Li_{10.42}Si/Ge_{1.5}P_{1.5}Cl_{0.08}O_{11.92}$ in the range between 27 °C and 110 °C. The activation energies for two types of solid electrolytes were calculated using the Arrhenius equation:

$$\sigma = A\exp(-E_a/kT) \quad (3)$$

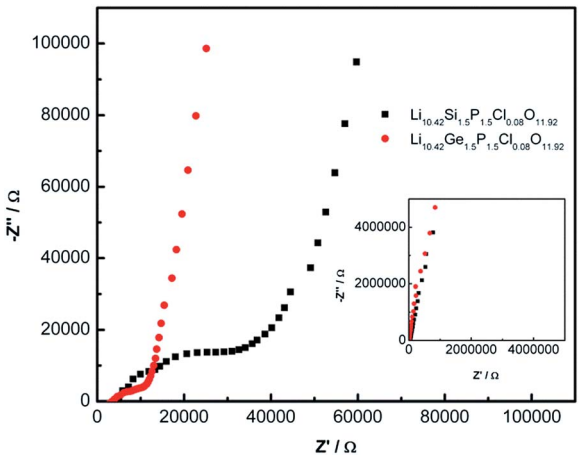

Fig. 1 Typical Nyquist plots of $Li_{10.42}Si_{1.5}P_{1.5}Cl_{0.08}O_{11.92}$ (square symbol) and $Li_{10.42}Ge_{1.5}P_{1.5}Cl_{0.08}O_{11.92}$ (circle symbol) measured at 27 °C.

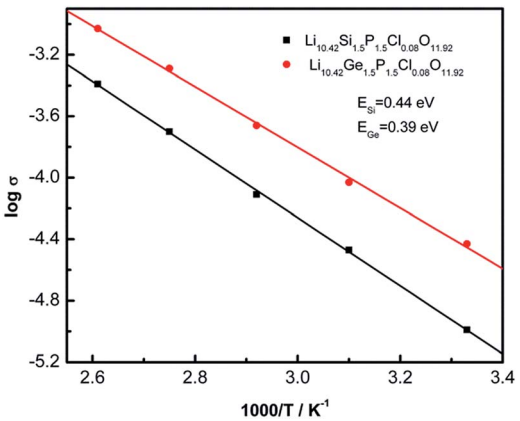

Fig. 2 Arrhenius plots of $Li_{10.42}Si/Ge_{1.5}P_{1.5}Cl_{0.08}O_{11.92}$ in the range between 27 °C and 110 °C.

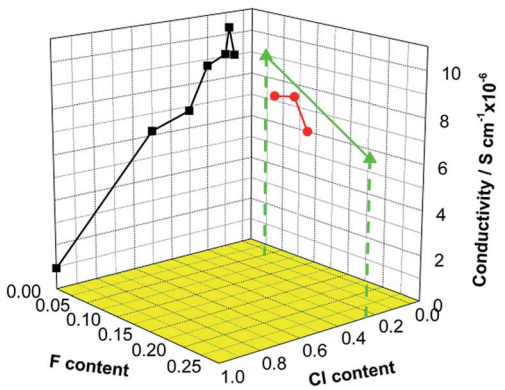

Fig. 3 Effect of halide substitution on the room-temperature conductivity of $Li_{10.5-x}Si_{1.5}P_{1.5}Cl/F_xO_{12-x}$ ($0.05 \leq x \leq 1.0$).

where A represents the pre-exponential factor, k is the Boltzmann constant, and T is the absolute temperature. The activation energy E_{Si} ($Li_{10.42}Si_{1.5}P_{1.5}Cl_{0.08}O_{11.92}$) and E_{Ge}

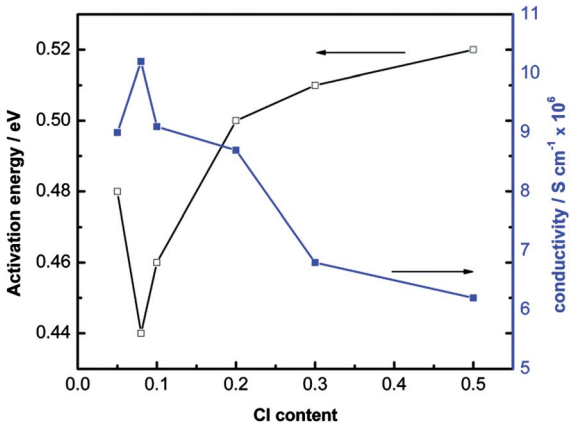

Fig. 4 The plots of room-temperature conductivity and activation energy *versus* Cl content.

($Li_{10.42}Ge_{1.5}P_{1.5}Cl_{0.08}O_{11.92}$) for the conduction was calculated to be 0.44 eV and 0.39 eV, respectively, which is much lower than that of the pristine $Li_{10.5}Si_{1.5}P_{1.5}O_{12}$ ($\approx$0.53 eV).[16]

Fig. 3 shows the effect of halide substitution on the room-temperature conductivity of $Li_{10.5-x}Si_{1.5}P_{1.5}Cl/F_xO_{12-x}$ ($0.05 \leq x \leq 1.0$). The square symbol displays the conductivity variation with substitution of Cl for O. A maximum conductivity $\sigma_{Li} \approx 1.03 \times 10^{-5}$ S cm^{-1} was found for $x = 0.08$. The solid circle symbol displays the conductivity variation with substitution of F for O. The maximum conductivity $\sigma_{Li} \approx 7.6 \times 10^{-6}$ S cm^{-1} was lower than their Cl counterpart, while the conductivities of $Li_{10.4}Si_{1.5}P_{1.5}Cl_{0.05}F_{0.05}O_{11.9}$ and $Li_{10}Si_{1.5}P_{1.5}Cl_{0.25}F_{0.25}O_{11.5}$ (triangular symbol) are comparable with their Cl counterpart $Li_{10.4}Si_{1.5}P_{1.5}Cl_{0.1}O_{11.9}$ and $Li_{10}Si_{1.5}P_{1.5}Cl_{0.5}O_{11.5}$. Whereas, the conductivities of $Li_{10.4}Si_{1.5}P_{1.5}Cl_{0.05}Br_{0.05}O_{11.9}$ is much lower ($\approx 7.4 \times 10^{-6}$ S cm^{-1}, not shown in this paper).

It is worth noting that the activation energy *versus* Cl content displays an inverted peak with the conductivity (Fig. 4). The lowest activation energy observed in the composition of $Li_{10.42}Si_{1.5}P_{1.5}Cl_{0.08}O_{11.92}$ that had the highest ionic conductivity.

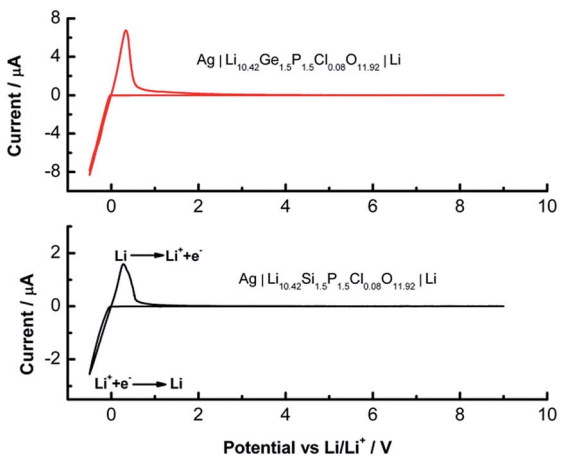

Fig. 5 The current–potential curves of $Li_{10.42}Si/Ge_{1.5}P_{1.5}Cl_{0.08}O_{11.92}$.

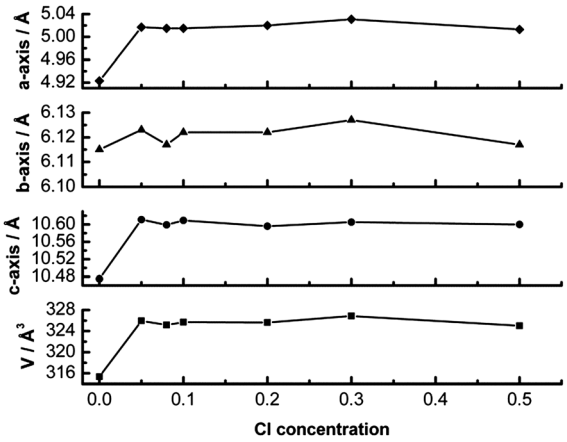

Fig. 6 The lattice constants and volume of unit cell of pure Li_3PO_4 and Cl-substituted $Li_{10.5-x}Si_{1.5}P_{1.5}Cl_xO_{12-x}$ solid solutions.

A high conductivity is necessary but not a sufficient property to make an electrolyte to be useful in practical terms. A wide electrochemical window is also an essential parameter to ensure good performance in rechargeable lithium batteries. The electrochemical stability window has been evaluated by running a cyclic voltammogram of cells, in which Li and Ag serve as reference/counter and working electrodes, respectively. Fig. 5 displays the current–potential curve of $Li_{10.42}Si/Ge_{1.5}P_{1.5}Cl_{0.08}O_{11.92}$. First, the potential was swept from open voltage (OCV) to −0.5 V (cathodic sweep) and then from −0.5 V to 9 V (anodic sweep). The cathodic current corresponding to lithium deposition, and the anodic current corresponding to lithium dissolution. No obvious current was observed except the ones due to

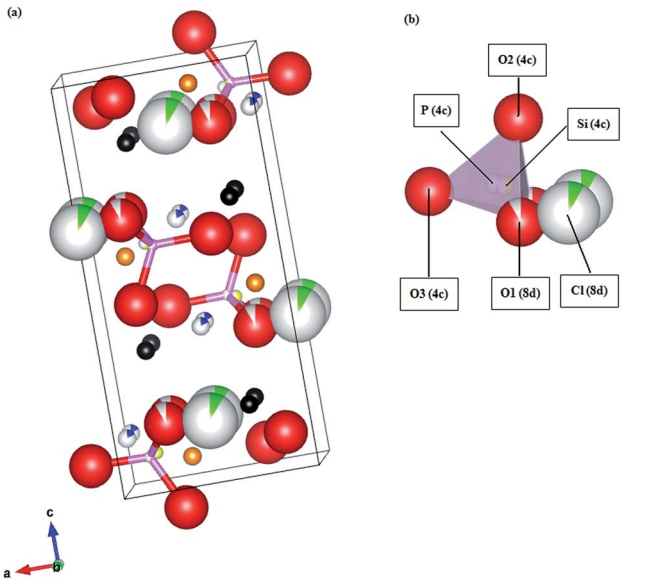

Fig. 7 (a) Ball and stick drawing of unit cell of $Li_{10}Si_{1.5}P_{1.5}Cl_{0.5}O_{11.5}$. (b) Enlarged view of the selected P/SiO/Cl_4 polyhedra. Li1 ions: black spheres, Li2 ions: orange spheres, Li3 ions: blue spheres, P ions: pink spheres, Si ions: yellow spheres, O ions: red spheres, Cl ions: green spheres.

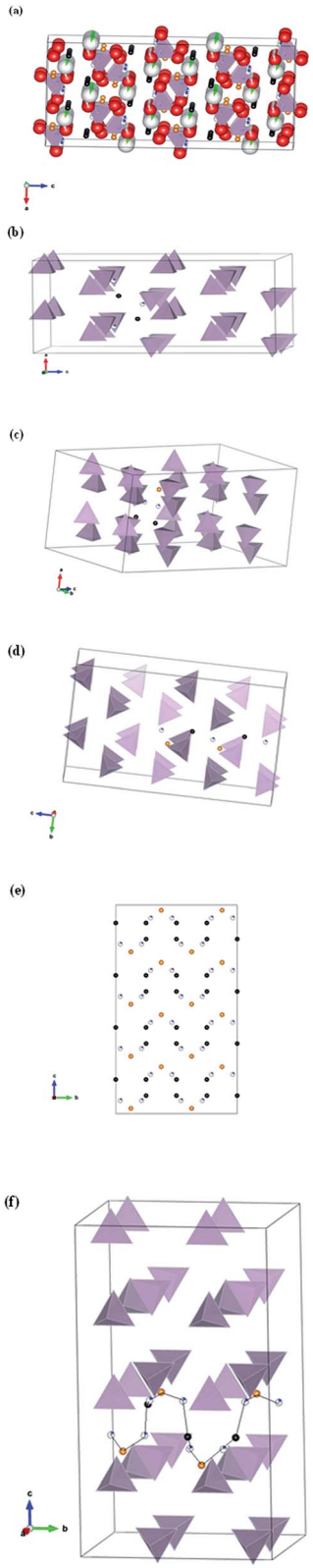

Fig. 8 (a) Polyhedra drawing of supercell of $Li_{10}Si_{1.5}P_{1.5}Cl_{0.5}O_{11.5}$ having dimension $2a \times 2b \times 2c$. (b)–(d) Lithium ions diffusion path along a–c axis, (e) projection of Li sites of supercell of $Li_{10}Si_{1.5}P_{1.5}Cl_{0.5}O_{11.5}$ on the $b \times c$ plane, (f) lithium ions diffusion path along $a \times b \times c$ axes.

Table 1 Interstitial migration step of $Li_{10}Si_{1.5}P_{1.5}Cl_{0.5}O_{11.5}$ solid solution

Net direction	Step	Net distance/Å
a	Li3(0.76472, 0.71260, 0.31232)	1.76, 2.37, 1.76, 2.37
	Li1(0.60328, 0.75030, 0.33631)	
	Li3(0.51472, 0.78740, 0.43768)	
	Li1(0.35328, 0.74970, 0.41369)	
	Li3(0.26472, 0.71260, 0.31232)	
b	Li3(0.51472, 0.28740, 0.43768)	2.0, 2.0
	Li2(0.66414, 0.37500, 0.47482)	
	Li3(0.51472, 0.46260, 0.43768)	
c	Li3(0.48528, 0.53740, 0.56232)	2.0, 2.82, 2.37, 2.0, 2.82, 2.37
	Li2(0.33586, 0.62500, 0.52518)	
	Li1(0.35328, 0.50030, 0.41369)	
	Li3(0.26472, 0.53740, 0.31232)	
	Li2(0.41414, 0.62500, 0.27518)	
	Li1(0.39672, 0.50030, 0.16369)	
	Li3(0.48528, 0.53740, 0.06232)	

the lithium deposition and dissolution, indicating that the $Li_{10.42}Si/Ge_{1.5}P_{1.5}Cl_{0.08}O_{11.92}$ electrolytes have a wide electrochemical window up to 9 V *vs.* Li^+/Li. $Li_{10.42}Si/Ge_{1.5}P_{1.5}Cl_{0.08}O_{11.92}$ would be an alternative for stable protective solid electrolyte interphase and buffer film taking into account their excellent electrochemical stability with lithium metal and promising ionic conductivities.

All XRD patterns of $Li_{10.5-x}Si_{1.5}P_{1.5}Cl_xO_{12-x}$ ($0.05 \leq x \leq 0.5$) (Fig. S1†) show that the matrix of Cl substitution is in the solid solution with structure of γ-Li_3PO_4 (Powder Diffraction File 15-0760, space group *Pnma*). The orthorhombic structure of γ-Li_3PO_4 widely used as a host for preparing lithium solid electrolytes. In particular, the LPON, LISICON and thio-LISICON electrolyte materials based on γ-Li_3PO_4 structure have been well developed.[17–19] Two different structures have been recognized in the system of solid solutions between Li_3PO_4 and Li_4SiO_4: the Li_4SiO_4-type phase and γ-Li_3PO_4-type phase with respective formulae of $Li_{4-x}Si_{1-x}P_xO_4$ ($0 \leq x \leq 0.12$) and $Li_{3+y}Si_yP_{1-y}O_4$ ($0 \leq y \leq 0.42$).[20] In the Li_4SiO_4-type phase, vacancies can be introduced into the normal Li^+ sites in the Li_4SiO_4 structure, while in the γ-Li_3PO_4-type phase, interstitial Li^+ can be introduced into the γ-Li_3PO_4 structure. In the system, $x = y = 0.5$, it shows γ-Li_3PO_4-type phase judged from the XRD patterns (Fig. S1†), indicating an interstitial ion migration mechamism.

The crystal structure of Cl-substituted $Li_{10.5-x}Si_{1.5}P_{1.5}Cl_xO_{12-x}$ ($0.05 \leq x \leq 0.5$) was analyzed by the Rietveld method.[21] The structure model of orthorhombic γ-Li_3PO_4 was adapted as the initial structure model with space group of *Pnma* (no. 62).[22] Typical observed, calculated, and difference patterns for Rietveld refinement of $Li_{10}Si_{1.5}P_{1.5}Cl_{0.5}O_{11.5}$ were shown in Fig. S2.† Table S1† lists the crystallographic data and details of the structure refinement. The resultant *R*-values reached $R_{wp} = 0.0787$, $R_p = 0.0638$. The Li1, Li2, Li3, P, Si, O1, O2, O3, Cl sites were the special positions of 8d, 4c, 8d, 4c, 4c, 8d, 4c, 4c, and 8d sites (the multiplicity and Wyckoff letter), respectively. The lattice constants were refined to be $a = 5.012(7)$ Å, $b = 6.116(6)$ Å, $c = 10.599(8)$ Å.

Fig. 6 shows the lattice constants and volume of unit cell of pure Li_3PO_4 and Cl-substituted $Li_{10.5-x}Si_{1.5}P_{1.5}Cl_xO_{12-x}$ solid solutions. The lattice constants and volume of unit cell of Cl-substituted $Li_{10.5-x}Si_{1.5}P_{1.5}Cl_xO_{12-x}$ solid solutions are much larger than the pure Li_3PO_4,[22] while the lattice constants and volume of unit cell vary very slightly when Cl concentration increases further, since the ionic radius of Cl^- (1.81 Å) is much larger than that of O^{2-} (1.4 Å).[11] There are no simple correlation between lattice constants and ionic radii.[23] Addressing the concept of bottleneck size and binding energy between mobile ions and the network anions, substitution of Cl for O increases the lattice constants and volume of unit cell, would enlarge the bottleneck size, then decrease the energy barriers (activation energy) and enhance the ionic conductivity. On the other hand, the ionicity of Li–Cl is smaller than that of Li–O due to the lower electronegativity of Cl^- (3.16) than O^{2-} (3.44). As the increase of Cl concentration, the Li^+ cations would be rigidly bonded to the Cl^- anions, which behaves as an obstacle for the ions migration, and increases the activation energy and decreases the ionic conductivity. Hence there should be an optimized Cl concentration with considerably large bottleneck size for Li^+ ions migration and relatively small binding energy between Li–O/Cl, which may lead to the minimum activation energy and maximum ionic conductivity (Cl = 0.08). This has been demonstrated in Fig. 4.

Fig. 7(a) illustrates the unit cell of $Li_{10}Si_{1.5}P_{1.5}Cl_{0.5}O_{11.5}$. In an ideal crystal of γ-Li_3PO_4, the Li ions are located at two different crystallographically sites indicated with Li1 and Li2, using the Wyckoff labels, 8d and 4c, respectively. The d site accounts for 8 equivalent atomic sites, and the c site accounts for 4 equivalent atomic sites per unit cell. The O ions fully occupy three different sites designated as O1(8d), O2(4c) and O3(4c), and the P ions fully occupy the 4c sites. Since in an ideal crystal, all the lithium cations fully occupy their positions and are rigidly bonded to the framework, which creates no prerequisites for ion migration. In the real crystal of $Li_{10}Si_{1.5}P_{1.5}Cl_{0.5}O_{11.5}$, Si and P ions share the same 4c sites due to partially substitution of Si for P (Fig. 7(b)). Noted that one site can just accommodate one atom, the P and Si ions cannot appear at 4c site at the same time, designating as white and pink spheres for P ions, and white and yellow spheres for Si ions in Fig. 7(b), indicating that they are

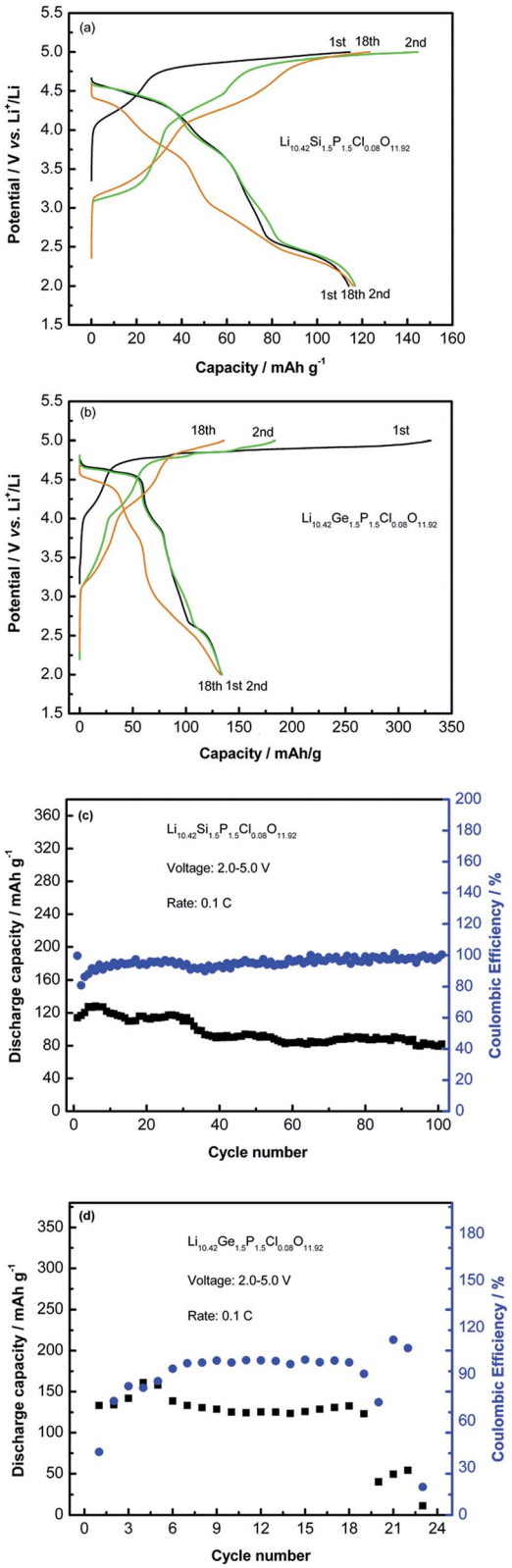

Fig. 9 (a) The charge–discharge curves of $Li_{10.42}Si_{1.5}P_{1.5}Cl_{0.08}O_{11.92}$ and (b) $Li_{10.42}Ge_{1.5}P_{1.5}Cl_{0.08}O_{11.92}$ cells at 0.1 C rate. (c) Cycle performance of $Li_{10.42}Si_{1.5}P_{1.5}Cl_{0.08}O_{11.92}$ cells. (d) Cycle performance of $Li_{10.42}Ge_{1.5}P_{1.5}Cl_{0.08}O_{11.92}$ cells.

occupied by P or Si exclusively. Cl and O ions share the same 8d sites due to partially substitution of Cl for O (Fig. 7(b)), designating as white and green spheres for Cl ions, and white and red spheres for O1 ions in Fig. 7(b), indicating that they are occupied by Cl or O exclusively. It is difficult to determine the exact positions of Cl ions due to their minor content and volatilization during preparation procedure. In the present work, we refine the crystal structure according to O1 sites occupied by Cl ions, and getting a reasonable agreement factors R_{wp} and R_p. However, the case that other O sites were occupied by Cl ions is also possible. 1.33 interstitial Li ions were introduced into unit per cell in the system of $Li_{10}Si_{1.5}P_{1.5}Cl_{0.5}O_{11.5}$. There are two crystallographically inequivalent Li interstitial sites I and II, and four sites equivalent to I site and eight sites equivalent to II site.[24] We firstly refine the crystal structure according to I site occupied by interstitial Li ions. However, it is unreasonable with the distance of 0.79 Å between interstitial Li ions and the neighbor O ions (not shown in this paper). Therefore, we supposed that the 1.33 interstitial Li ions occupy the interstitial II sites, designating as Li3 in Fig. 7 (white and blue spheres).

Interstitial migration of the lithium ion were showing in dimension $2a \times 2b \times 2c$ supercells in Fig. 8. The hypothesis of interstitial mechanism described here for ions diffusion within the type II voids suggest that possible mechanism for interstitial Li ion diffusion in all three crystallographic directions (Fig. 8(a)). We thus considered the possibly efficient diffusion path along the three crystallographic directions, by selecting shorter Li–Li distance to hop which indicating smaller migration barrier[24] tabulated in Table 1. Fig. 8(b) described diffusion of an interstitial Li ion Li3(0.76472, 0.71260, 0.31232) to its equivalent site Li3(0.26472, 0.71260, 0.31232) along *a* axis. During the motion process, an interstitial Li ion Li3(8d) kicks out and replaces a neighboring Li1(8d) while the "kicked-out" Li1(8d) migrates to next neighboring Li3(8d) site, then kicks out Li1(8d) to take its equivalent site Li3(0.26472, 0.71260, 0.31232). It takes four steps from one interstitial site to its equivalent site, and the shortest Li–Li distance is 1.76 Å, and the largest Li–Li distance is 2.37 Å. The diffusion path along *a* axis is (Fig. 8(b)):

$$\text{Li3(8d)} \rightarrow \text{Li1(8d)} \rightarrow \text{Li3(8d)} \rightarrow \text{Li1(8d)} \rightarrow \text{Li3(8d)} \quad (4)$$

The diffusion paths along *b* and *c* axis are similar with that along *a* axis, both are zigzag motions. The diffusion path along *b* axis is (Fig. 8(c)):

$$\text{Li3(8d)} \rightarrow \text{Li2(4c)} \rightarrow \text{Li3(8d)} \quad (5)$$

The diffusion path along *c* axis is (Fig. 8(d)):

$$\begin{aligned}\text{Li3(8d)} \rightarrow \text{Li2(4c)} \rightarrow \text{Li1(8d)} \rightarrow \text{Li3(8d)} \\ \rightarrow \text{Li2(4c)} \rightarrow \text{Li1(8d)} \rightarrow \text{Li3(8d)}\end{aligned} \quad (6)$$

The proposed diffusion paths show a slight anisotropy along the three crystallographic directions. Based on the diffusion steps from one interstitial site to its equivalent site and the Li–Li distance, it can be deduced that the diffusion path along *b* axis is the most efficient and major motion path of this solid

solution. Fig. 8(e) shows the projection of Li sites of supercell of $Li_{10}Si_{1.5}P_{1.5}Cl_{0.5}O_{11.5}$ on the $b \times c$ plane, which can visually deliver a zigzag diffusion path along b axis. Fig. 8(f) shows the 3D-zigzag network of lithium ions diffusion path along $a \times b \times c$ axes. The diffusion along b axis combined with the diffusion along $a \times c$ axes.

The cathode material $0.3Li_2MnO_3 \cdot 0.7LiMn_{1.5}Ni_{0.5}O_4$ which proves to be able to stably cycle in a wide potential window of 2.0–5.0 V has been adopted to evaluate the electrochemical performance of $Li_{10.42}Si_{1.5}P_{1.5}Cl_{0.08}O_{11.92}$ and $Li_{10.42}Ge_{1.5}P_{1.5}Cl_{0.08}O_{11.92}$. Fig. 9(a) and (b) show the charge–discharge curves of the hybrid electrolyte $Li_{10.42}Si_{1.5}P_{1.5}Cl_{0.08}O_{11.92}$ and $Li_{10.42}Ge_{1.5}P_{1.5}Cl_{0.08}O_{11.92}$ cells at 0.1 C rate. The charge and discharge capacities of $Li_{10.42}Si_{1.5}P_{1.5}Cl_{0.08}O_{11.92}$ cell at the 1st cycle were 114.5 mA h g^{-1} and 114.1 mA h g^{-1}, respectively, delivering almost 100% coulombic efficiency. The initial charge capacity of $Li_{10.42}Ge_{1.5}P_{1.5}Cl_{0.08}O_{11.92}$ cell was 330.1 mA h g^{-1}, much higher than the theoretical capacity of $0.3Li_2MnO_3 \cdot 0.7LiMn_{1.5}Ni_{0.5}O_4$ (213 mA h g^{-1}), whereas the initial discharge capacity was 133.2 mA h g^{-1}. The charge and discharge capacities after 100 cycles were 81.6 mA h g^{-1} and 81.9 mA h g^{-1}, respectively, with 100% coulombic efficiency for $Li_{10.42}Si_{1.5}P_{1.5}Cl_{0.08}O_{11.92}$ cells (Fig. 9(c)). However, the discharge capacity was 11.2 mA h g^{-1} for $Li_{10.42}Ge_{1.5}P_{1.5}Cl_{0.08}O_{11.92}$ cells after 23 cycles (Fig. 9(d)). The cycle performance of $Li_{10.42}Si_{1.5}P_{1.5}Cl_{0.08}O_{11.92}$ cells was much better than that of $Li_{10.42}Ge_{1.5}P_{1.5}Cl_{0.08}O_{11.92}$ cells.

Conclusions

To achieving the combination of high ionic conductivity and excellent electrochemical stability in lithium solid electrolytes still remains a major challenge. A facile strategy was proposed to achieve reasonably high conduction and excellent electrochemical stability by the substitution of Cl for O based on the concept of bottleneck size and binding energy. New electrolytes, $Li_{10.42}Si_{1.5}P_{1.5}Cl_{0.08}O_{11.92}$ and $Li_{10.42}Ge_{1.5}P_{1.5}Cl_{0.08}O_{11.92}$, were synthesized that showed promising ionic conductivity 1.03×10^{-5} S cm^{-1} and 3.7×10^{-5} S cm^{-1} at 27 °C respectively, 13 orders of magnitude higher than that of the pure Li_3PO_4, and 1 order of magnitude higher than that of the pristine $Li_{10.5}Si_{1.5}P_{1.5}O_{12}$, and superior electrochemical stability with metallic lithium up to 9 V *vs.* Li^+/Li, one of the solid electrolytes with most wide electrochemical window. These series of new electrolytes are orthorhombic structure of γ-Li_3PO_4 with interstitial 3D-zigzag ions migration mechanism along b axis. The charge and discharge capacities of $Li_{10.42}Si_{1.5}P_{1.5}Cl_{0.08}O_{11.92}$ cell at the 1st cycle were 114.5 mA h g^{-1} and 114.1 mA h g^{-1}, respectively, with almost 100% coulombic efficiency. The coulombic efficiency was almost 100% after 100 cycles for $Li_{10.42}Si_{1.5}P_{1.5}Cl_{0.08}O_{11.92}$ cells. This strategy holds promising potential to develop new solid electrolytes combined with high ionic conductivity and excellent electrochemical stability thus advance lithium ion battery technology by enabling the use of metallic lithium anode.

Acknowledgements

This work was supported by SERC 2011 Public Sector Research Funding (PSF) Grant R-265-000-424-305.

Notes and references

1 J. B. Goodenough and Y. Kim, *Chem. Mater.*, 2010, **22**, 587.
2 Z. C. Zhang, L. B. Hu, H. Wu, W. Weng, M. Koh, P. C. Redfern, L. A. Curtiss and K. Amine, *Energy Environ. Sci.*, 2013, **6**, 1806.
3 L. Suo, Y. S. Hu, H. Li, M. Armand and L. Q. Chen, *Nat. Commun.*, 2012, **4**, 1481.
4 R. Kanno and M. Maruyama, *J. Electrochem. Soc.*, 2001, **148**, A742.
5 N. Kamaya, K. Homma, Y. Yamakawa, M. Hirayama, R. Kanno, M. Yonemura, T. Kamiyama, Y. Kato, S. Hama, K. Kawamoto and A. Mitsui, *Nat. Mater.*, 2011, **10**, 682.
6 Y. Seino, T. Ota, K. Takada, A. Hayashi and M. Tatsumisago, *Energy Environ. Sci.*, 2014, **7**, 627.
7 G. Sahu, Z. Lin, J. Li, Z. Liu, N. Dudney and C. D. Liang, *Energy Environ. Sci.*, 2014, **7**, 1053.
8 J. L. Schaefer, Y. Lu, S. Moganty, P. Agarwal, N. Jayaprakash and L. A. Archer, *Appl. Nanosci.*, 2012, **2**, 91.
9 W. C. West, J. F. Whitacre and J. R. Lim, *J. Power Sources*, 2004, **126**, 134.
10 Y. Inagum and M. Itoh, *Solid State Ionics*, 1996, **86**, 257.
11 O. Bohnke, C. Bohnke, J. O. P. Ahmed, C. Lopez, H. Duroy, F. Berre and J. L. Fourquet, *Chem. Mater.*, 2001, **13**, 1593.
12 Y. Inaguma, Y. Matsui, J. Yu, Y. J. Shan, T. Nakamura and M. Itoh, *J. Phys. Chem. Solids*, 1997, **58**(6), 843.
13 H. Y. Hong, *Mater. Res. Bull.*, 1978, **13**, 117.
14 J. T. S. Irvine, D. C. Sinclair and A. R. West, *Adv. Mater.*, 1990, **2**, 132.
15 B. Wang, B. C. Chakoumakos, B. C. Sales, B. S. Kwak and J. B. Bates, *J. Solid State Chem.*, 1995, **115**, 313.
16 Y. W. Hu, I. D. Raistrick and R. A. Huggins, *J. Electrochem. Soc.*, 1977, **124**, 1240.
17 J. B. Bates, N. J. Dudney, G. R. Gruzalski, R. A. Zuhr, A. Choudhury, D. F. Luck and J. D. Robertson, *Solid State Ionics*, 1992, **647**, 53.
18 P. G. Bruce and A. R. West, *J. Electrochem. Soc.*, 1983, **130**, 662.
19 R. Kanno, H. Kawamoto and Y. M. Irie, *Solid State Ionics*, 2000, **130**, 97.
20 A. Khorassani, G. Izquierdo and A. R. West, *Mater. Res. Bull.*, 1981, **16**, 1561.
21 H. Xie, J. A. Alonso, Y. T. Li, M. T. Fern and J. B. Goodenough, *Chem. Mater.*, 2011, **23**, 3587.
22 W. Baur and H. T. Ohta, *J. Solid State Chem.*, 1982, **44**, 50.
23 R. Ubic and G. Subodh, *J. Alloys Compd.*, 2009, **488**, 374.
24 Y. A. Du and N. A. W. Holzwarth, *J. Electrochem. Soc.*, 2007, **154**, A999.

